Towards a holistic predesign approach using rotor cant of EVTOL aircraft

Pierre-Marie Basset, Jean-Paul Reddinger, Raphaël Perret, Nathan Beals, J Michael Vegh

TOWARDS A HOLISTIC PREDESIGN APPROACH USING ROTOR CANT OF EVTOL AIRCRAFT

Pierre-Marie Basset, ONERA – The French Aerospace Lab, Salon de Provence, France
Jean-Paul Reddinger, DEVCOM Army Research Laboratory, Salon de Provence, France
Raphaël Perret, ONERA – The French Aerospace Lab, Salon de Provence, France
Nathan Beals, DEVCOM Army Research Laboratory, Aberdeen Proving Ground, MD, USA
J. Michael Vegh, DEVCOM Aviation and Missile Center, Moffet Field, CA, USA

Abstract

Pre-design analysis of a Lift+Cruise eVTOL configuration was performed using cant as a primary design parameter in order to illustrate the need for a comprehensive approach during the conceptual design phase. Rotor rotation direction was also considered from design requirement and controllability perspectives and was found to follow the choice of cant angle direction. Rotor cant was shown to have an impact on performance, controllability, stability, safety, failure tolerance, and motor design requirements. Introducing cant was shown to cause minor penalties to hover power requirements resulting from changed orientation of thrust vectors and an increase in the design gross weight in exchange for resilience to two-engine-inoperative failures and significantly improved yaw control derivatives at low speeds, the addition of a purely translational lateral control axis, the ability to reduce the negative impact of blade breaks, and the potential to stabilize rigid-body modes that are unstable for an uncanted system.

1. INTRODUCTION

There is currently a rapid global growth in electric Vertical Take-Off and Landing (eVTOL) aircraft development driven by the anticipated use of low carbon footprint, quiet vehicles for Advanced Air Mobility transport applications. These aircraft are based on the paradigm of distributed electric propulsion with multiple lifting rotors often paired with fixed wings for better cruise efficiency. Novel configurations introduce challenges that require the adoption of new modeling and numerical analysis methodologies for predesign and sizing.

The main purpose of this paper is to illustrate the need for a holistic approach to predesign—which incorporates analyses that typically are not considered until later in the design process—and to further understand an emerging eVTOL configuration. As a concrete example, a subset of key design parameters will be investigated in detail, which includes the positions, rotation directions, and cant angles of the lifting rotors. The trade-offs of illustrative design choices are explored with the aim of identifying the types of analyses that are most impactful, and developing guidelines that can be used to facilitate the predesign of future eVTOL configurations. The paper will evaluate the importance of the following within predesign phase:

1. Steady, trimmed flight performance throughout the aircraft's flight envelope, including through transition between VTOL and airplane modes,
2. Stability and controllability characteristics in hover with and without lateral relative wind,
3. Safety and comfort considerations of the pilot and passengers, and
4. Failure of one or more thrust generation systems (ESC/motor/rotor).

Additional criteria that are not examined in this paper but could be impactful with respect to cant angle include: rotor wake effects on ground particles projection on the aircraft, in-ground-effect (IGE) stability and

dynamics, acoustics, and structural dynamics. Furthermore, aerodynamic interactions between rotary wings and fixed wings are influenced by cant angles, and a thorough analysis would require a dedicated paper. Some of the aforementioned criteria can be considered as constraints, others as objectives in a global multi-domain optimization (MDO) problem addressing the trade-off between efficiency, safety, acceptability, affordability, etc. This paper does not intend to show a solution of the MDO problem, but to illustrate the need for multi-domain analysis in the design of such configurations.

2. APPROACH

2.1. Vehicle Description

The Lift+Cruise (L+C) configuration studied in this paper is based on the SLC (Separate Lift and Cruise) eVTOL configuration defined and outlined in Ref. 1 and shown in Figure 1. The L+C configuration is a high wing aircraft with rudders integrated into the boom mounts of the inner lifting rotors. For controls, the aircraft uses 13 RPM-controlled fixed-pitch rotors, 12 of which are lifting rotors and one of which is a thrusting pusher propeller. In addition, the aircraft includes 5 fixed-wing control surfaces: a flaperon on each of the main wings, a rudder on each of the two fins, and one elevator on the horizontal stabilizer. In total, this aircraft possesses 18 independent control actuators.

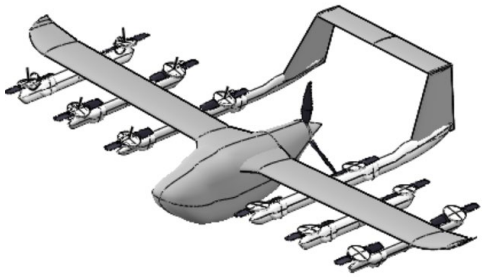

Figure 1: 3D model of the Lift + Cruise configuration

The baseline aircraft mass used for the analysis in this paper is a prescribed 1200 kg, with a lateral and longitudinal location of the center of gravity assumed to be coincident with the geometric centroid of the 12 lifting rotors. This assumption produces the most generalizable results and is expected to require the lowest power to trim in hover.

The L+C configuration introduces two degrees of complexity not typically encountered during the conceptual design phase of conventional rotorcraft. First, the 18 controls provide a high degree of control redundancy that produces potentially infinite feasible trim solutions. Secondly, the design problem is multi-domain to a degree not typically encountered in traditional rotorcraft. For example, different cant angles can be used on the 12 lifting rotors. This complexity could add cost and time if design decisions are not addressed at the earliest stages.

To study the first-order effects of the cant angles, a baseline uncanted configuration is defined with all 12 lifting rotors in a horizontal position thrusting in the same direction as introduced in Ref. 2. A series of alternative canted versions of the baseline L+C configuration introduce different cant angles for each of the three sets of inner, middle, and outer lifting rotors as shown in Figure 2. These cant angles orient the thrust towards the centerline (dihedral), towards the wing tips (anhedral), or a combination thereof (canted). Notably, the rotation direction of each lifting rotor must also be modified to ensure the lateral thrust component produces a yaw moment which is additive with reaction torque about the center of gravity. This design decision will be further explained in Section 3.3.

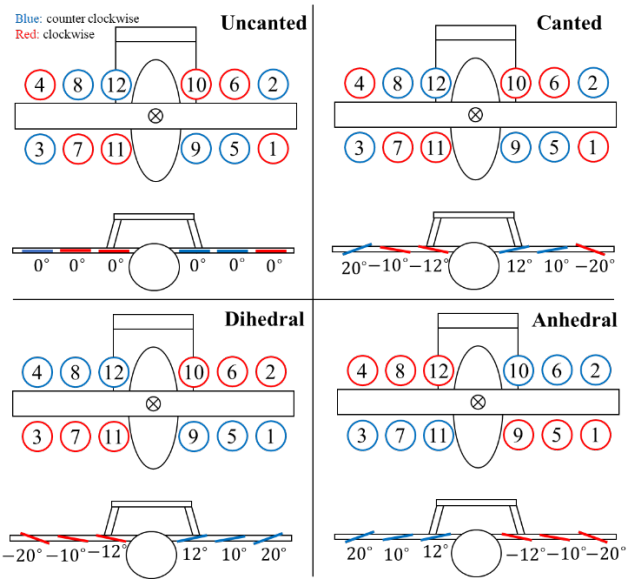

Figure 2: Top and front view diagrams of the lift + cruise configuration showing four sets of spin direction and cant angles.

This paper intends to demonstrate capability gaps in methods and models by studying the trade-off between the impacts of these choices at early design stages. In the absence of experimental data on these emerging configurations, the approach is to compare the results between the different tools of the three collaborating organizations. First, the conceptual design tools will be briefly described. Then examples of results will be shown from these different points of view: performance, stability, controllability, safety and failure resilience, and impact on weight assessment.

2.2. Modeling and predesign tools

A predesign version of this Lift+Cruise aircraft was developed and modeled in each of three tools based on a common set of sizing criteria defined in Ref. 1. These tools used in this study are identical to those described in Ref. 1, and will be summarized below:

C.R.E.A.T.I.O.N. (Concepts of Rotorcraft Enhanced Assessment Through Integrated Optimization Network) is the ONERA numerical workshop dedicated to the VTOL conceptual studies and evaluation at early predesign stages (Refs. 3-5). The main tool within the CREATION workshop used for this study is DynaPyVTOL, a comprehensive analysis tool for flight dynamics simulation of any aircraft developed and maintained at ONERA. DynaPyVTOL is used to perform trim and linearization. This software is predominantly written in Python, while blade-element momentum theory rotor calculations are performed in a Fortran sub module and empirically corrected based on a higher-order free-wake model ("Aero-Multi-Body" AMB, see Ref. 3) to account for aerodynamic interaction effects.

NDARC (NASA Design and Analysis of RotorCraft) is a conceptual level tool developed by NASA and in use by DEVCOM AvMC along with other government, academic, and private industry organizations (Ref. 6). NDARC uses parametric and semiparametric component-based weight and performance models to estimate the performance and weight of a variety of diverse configurations. Rotor performance models were calibrated to CAMRAD II analysis as documented in Ref. 1 and 7. Examples of using this code for Lift+Cruise configuration along with documentation of the approach can be seen in Refs. 1,8, and 9.

HYbrid Design and Rotorcraft Analysis (HYDRA) is a conceptual design and performance code originally created at the University of Maryland—College Park which is now in use and development by DEVCOM

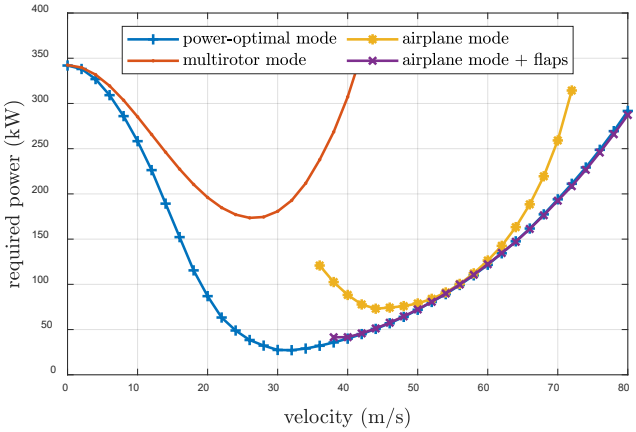

Figure 3: Comparison of trim strategies and the impact on trimmed power requirement for the uncanted configuration.

Army Research Laboratory (Ref. 10). HYDRA has been developed primarily for small to mid-size (US Department of Defense Groups 1-3) Unmanned Aircraft Systems (UAS). HYDRA uses empirical, semi-empirical, and physics-based (Ref. 11) subsystem weight models along with an optimization-based trim routine (Ref. 12) to size and predict the performance of nearly arbitrary UAS concepts.

3. RESULTS

3.1. Performance

Trim of Overactuated Systems

Traditionally, optimizing for performance subject to additional anticipated requirements is a primary design goal of the sizing and predesign phase, with range and endurance as common performance objectives. For these reasons, performance will be treated as a baseline consideration against which the impacts of the rest will be compared.

Initial trim analysis was conducted using DynaPyVTOL to investigate the uncanted configuration. Control redundancy requires either a subset of controls to be used for equilibrium or formulating trim as an optimization problem. Figure 3 compares the power requirement in trim with several subsets of trim variables:

1. **Power-optimal Mode:** Trim using all controls and pitch attitude to minimize the total required power.
2. **Multirotor Mode:** Includes the collective (δ_{col}), longitudinal (δ_{lon}), lateral (δ_{lat}), and pedal (δ_{ped}) controls, as well as pitch attitude for a unique trim

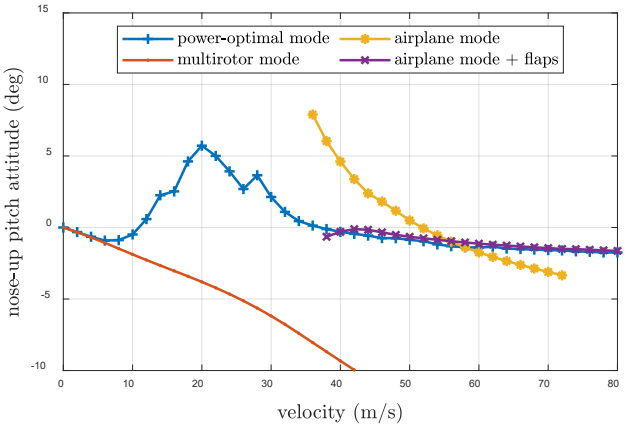

Figure 4: Comparison of trim strategies and the impact on trimmed pitch attitude for the uncanted configuration.

solution at each flight speed—differential rotor controls (outer/middle/inner) are ignored.

3. **Airplane Mode:** Fixed wing control surfaces and pusher propeller, including differential flaperons (δ_{ail}), elevators (δ_{ele}), rudder (δ_{rud}), and propeller thrust (δ_{prop}).

4. **Airplane Mode + Flaps:** An augmented set of fixed wing controls with control redundancy due to the addition of collective flaperons (δ_{flap}).

From this analysis the following observations were made:

- Power-optimal trim at 40 m/s and over is attained with zero rotor RPM, using only the fixed wing controls with the collective flaperons. This can be attributed to the loss of control sensitivity to rotors with low disk loading as well as the lifting efficiency of wings compared to rotors.

- Hover and low speed trim (under 5 m/s) solved with just the lifting rotors in multirotor mode is approximately equivalent to power-optimal trim. This is due to the lack of dynamic pressure necessary to generate control moments with the fixed wings.

- There is a difference between using the differential flaperons only (roll control only) vs. using differential and collective mode (lift or heave control), which is impacted by the relative difference between the fuselage drag sensitivity to pitch and the flaperon drag sensitivity to control surface deflection. This is further demonstrated in the difference between the trimmed pitch attitudes of these two control modes in Figure 5.

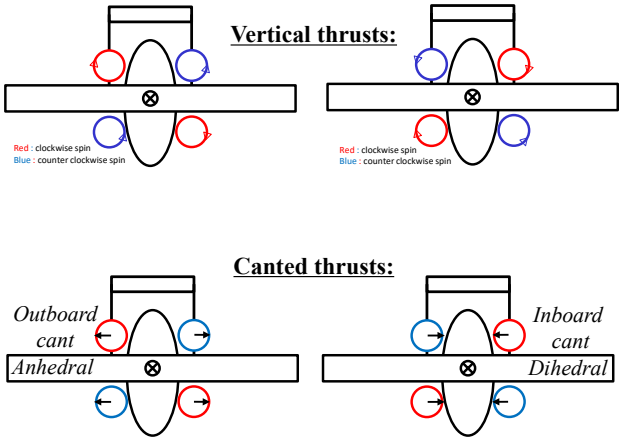

Figure 5: Lifting rotors direction of rotation in the case of zero cant angles or with cant angles.

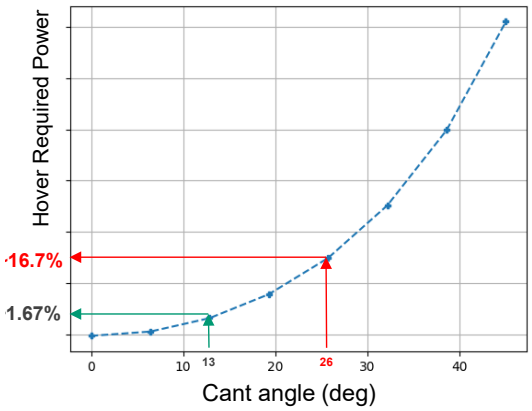

Figure 6: Increase in hover required power with cant angle on a simplified quad lift + cruise configuration.

- The transition region, between VTOL and Airplane modes, is between 5 and 40 m/s. Figure 5 shows that the power optimal solution for transition exhibits non-monotonic pitch behavior with increasing flight speed, and peaks with a nose-up pitch attitude in excess of 5° at 20 m/s.

Impact of Canted Rotors

For power-optimal trim of the uncanted configuration in hover, each of the 12 horizontal lifting rotors will produce the same 981 N of thrust obtained with the same RPM. In the case of the canted configuration, an optimal trim algorithm minimizing power requirements gives an optimal thrust distribution with three different thrusts for each of the three groups of canted rotors in Figure 2. The closer to horizontal the rotor, the more evenly distributed the thrust among the rotors. This is because the lateral components of the

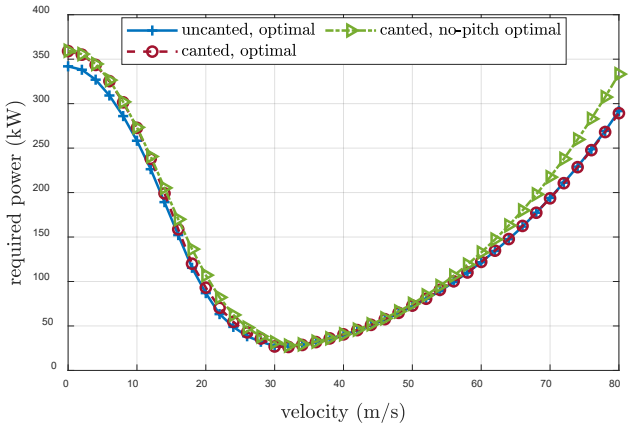

Figure 7: Comparison of impact of cant and aircraft pitch attitude constraint on power requirement.

thrust will cancel out between the right and left sets of rotors, while only the vertical component offsets weight. It is therefore more efficient overall to shift the lift-share to the most horizontally-aligned rotors.

When the optimal trim is computed to minimize the total required power, the thrust of one rotor in each of the three canted groups is:

- Outer (-20° cant): 955.15 N
- Middle (10°cant): 1049.06 N
- Inner (12° cant): 1034.92 N

Figure 5 shows a simplified configuration with only 4 lifting rotors instead of 12 and the same symmetrical inboard or outboard cant angles. For two configurations shown, the required power for hover increases with the cant angles, as demonstrated in Figure 6.

The power increase is non-linear such that the power requirement increases by 1.7% with 13° of cant relative to the uncanted case (0°). Doubling the cant from 13° to 26° further increases the required power by a factor of 10 (17% higher than the uncanted case).

For the 12-rotor configuration, Figure 7 compares the performance impact of the canted L+C configuration against the baseline uncanted L+C configuration (Figure 2) when optimized for minimum power over the entire flight speed domain. The impact of the cant is a 5% increase in hover power requirement (17 kW). This difference diminishes with increased flight speed until 32 m/s, after which point the rotors are offloaded, and there is no significant impact of canting.

In summary, the power penalties of canting primarily impact hover and low speed flight and grow non-linearly with increased cant. The benefits of canting must be weighed against these penalties. If the benefits of canting the lifting rotors can be obtained with low cant angles and the aircraft is not designed for significant hovering and vertical flight missions, then cant may provide the benefits outlined in the following sections.

3.2. Pilot & Passengers Comfort

Figure 4 shows that trimmed aircraft pitch attitude behaves non-linearly through transition. A free pitch attitude allows the aircraft to pitch nose up during transition, increasing the lift generated by the wing and reducing the power requirement between 15 and 30 m/s. However, following such a trim schedule may be counter-intuitive to a pilot since pitch first increases and then decreases through transition.

One additional trim sweep can be performed to quantify the performance penalty if the pitch attitude is fixed. In Figure 7, the power penalty for fixing the pitch attitude to a constant value (0° in this case) for all flight speeds is shown. Based on these results, there is little power penalty but potentially large impacts on pilot and passenger comfort when removing pitch attitude from trim and control strategies.

The power increase (relative to the canted optimal case) is limited to transition and high speed. This increase depends on the drag sensitivity to pitch attitude and control deflection which may not be easy to assess at the early design stages of these new configurations due to a dependance on boom and stopped rotor drag. This requires engineering judgement and evaluation of how to compare the relative benefits of range, endurance, and pilot comfort depending on the eVTOL mission.

3.3. Control Authority

The direction of rotation for the lifting rotors must be such that rolling or pitching commands do not induce yaw. This imposes the requirement that on each side (right/left for roll symmetry or front/aft for pitch symmetry), there must be the same number of identical lifting rotors turning in opposite directions in order for their torques to produce yaw equilibrium. On a simplified configuration with 4 lifting rotors without cant, the direction of rotation must be one of the two options in Figure 5.

With cant angles introduced, the direction of rotation introduces a yaw coupling of the thrust with the reaction torque about the center of gravity. Therefore, the spin direction that produces a thrust yaw moment compatible with the rotor reaction torque is subject to

the cant angle and rotor location. This impacts the pedal control derivative in either an additive or subtractive manner. This effect has been observed in both analysis and experiment (Refs. 13, 14). Therefore, a design constraint can be imposed to prevent loss of pedal control, such that thrust and reaction torque can only be additive (see Figure 4 with Canted Thrusts).

One method of comparing the control authority can be done by examining the Attainable Control Set (ACS). ACS analysis figures provide a three-dimensional volume that represents the domain of accelerations reachable by a trimmed aircraft on its 6 rigid body degrees of freedom when making variations in each control to each limit. The results depend on these control ranges (e.g., minimum and maximum RPM), which are parameters that may not yet be known in the pre-design phase. Yet by comparing the ACS of two identical configurations (same control ranges, rotors etc.), the effect of a design parameter (for example, cant angle) can be assessed in a relative sense.

Figure 8 demonstrates the use of ACS on the simplified quadrotor configuration from Figure 5 with both zero cant and 5° of cant (which additively couples the torque and thrust contribution to yaw moment about the center of gravity). When compared with the uncanted case (ACS in black), the ACS with cant angles in blue are clearly larger in the yaw axis, while remaining relatively unchanged in roll and pitch.

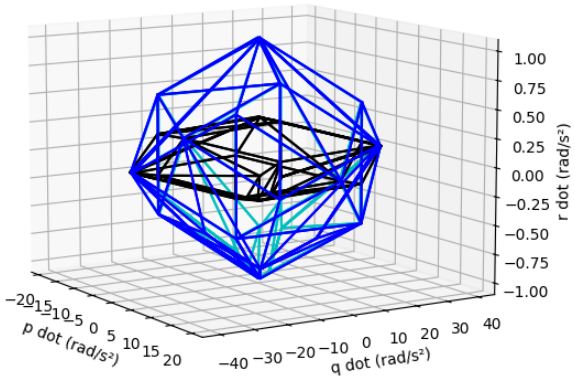

Figure 8: ACS in hover of a quad LiftCruise Black no cant, Blue + 5°, Cyan -5°.

The maximum attainable yaw acceleration ($\dot{r} = dr/dt$) is significantly increased by using canted lifting rotors (+/-5°) when compared with the uncanted case in black. Relative values rather than absolute values must be considered since absolute values depend on control range assumptions, dimensions, etc. The canted configurations with only (+/-5°) produce a factor near 3 on the maximum yaw acceleration with respect to the uncanted case. With a cant angle of 13° (Figure 9), the maximum yaw acceleration is multiplied by a factor 7 with respect to the uncanted configuration. If the direction of cant angle of the 4 lifting rotors is not compatible with their reaction torques, this factor is reduced to 4 with 13° of cant.

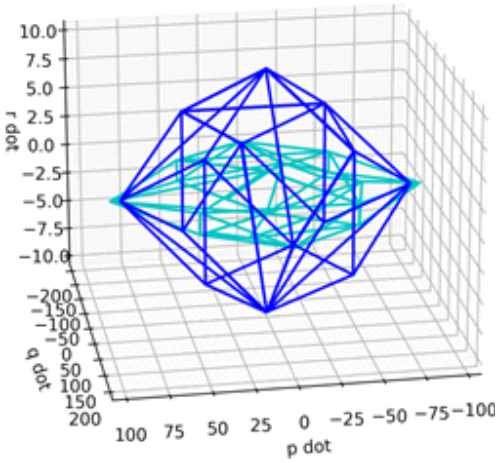

Figure 9: ACS in hover of a quad LiftCruise Blue + 13° of cant, Cyan no cant.

In addition to this significant positive effect on the yaw authority, the cant angles also bring the capacity to generate lateral acceleration ($\dot{v} = dr/dt$) without using bank or roll attitude angle. The ACS in Figure 10 illustrates this positive effect. In horizontal hovering flight, the uncanted configuration has no lateral acceleration capability, whereas the canted configuration with 5° of outboard canting exhibits the ACS on Figure 10. The more the cant angle increases, the more its lateral acceleration in horizontal attitude increases. This will be also viewed from a safety perspective hereafter by considering hovering close to the ground with a lateral wind.

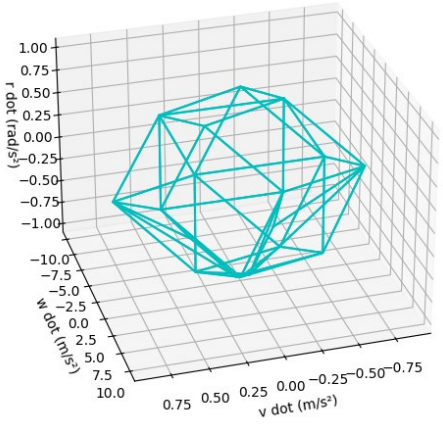

Figure 10: ACS in Hover for a quad configuration with 5° outboard canted lift rotors.

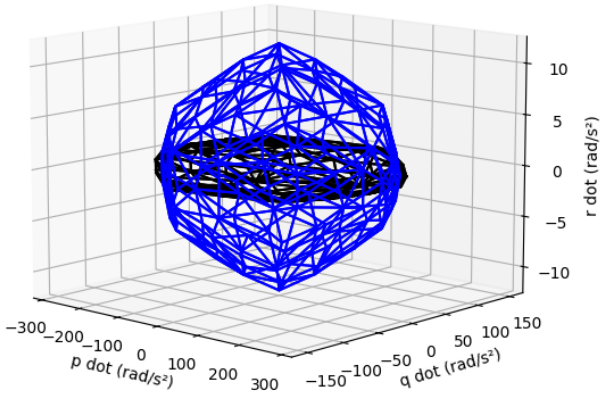

Figure 11: horizontal hover, ACS rotation accelerations comparisons between the uncanted in black and the canted L+C in blue.

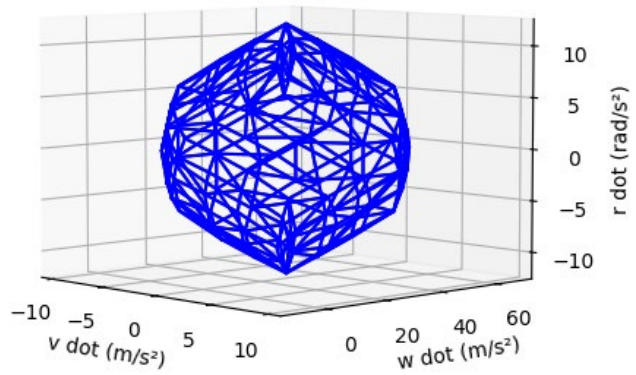

Figure 12: ACS on lateral, vertical and yaw accelerations of the canted L+C in horizontal hover.

ACS comparisons between the canted and uncanted Lift+Cruise configuration with 12 lifting rotors canted differently (Figure 2) show similar results.

Figure 11 shows the improvement of the yaw acceleration capability brought by the canting of the lifting rotors. There is a factor about 4.77 between the maximum yaw acceleration of the canted configuration compared to the uncanted configuration. Small differences are observed on the roll and pitch accelerations. With its slightly higher vertical thrusts, the uncanted configuration can produce slightly higher heave, roll and pitch accelerations (3.8% more on vertical acceleration, 3.7 % more on roll and 5 % more on pitch). But these secondary effects remain negligible compared to the two main improvements in terms of acceleration (or forces and moments) capability brought by canting the lifting rotors:

- An improved yaw acceleration (in relative value, the uncanted configuration has about 80% less yaw acceleration capacity),
- An additional lateral motion capability (degree of freedom or control mode): the L+C canted configuration can generate lateral acceleration (or forces) without any roll or bank angle of the aircraft.

The uncanted L+C is not able to produce lateral forces without laterally tilting the whole aircraft, whereas the canted configuration can produce lateral forces and acceleration even in horizontal attitude as illustrated on the ACS shown in Figure 12.

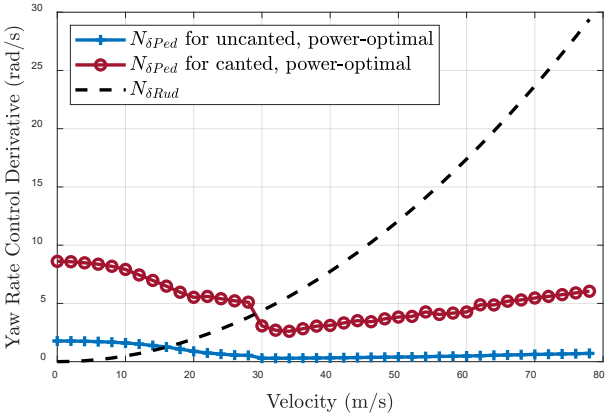

Figure 13: yaw authority comparison between the canted and uncanted configurations.

Another means to assess the control authority is to compare the control sensitivity terms of the [B] matrix of the linearized model about each trim state and not only in hover. For the Lift+Cruise configuration with 12 lifting rotors (Figure 2), Figure 13 shows the difference between the linearized yaw control derivative with respect to the normalized pilot pedal command ($N_{\delta Ped}$) and normalized rudder command ($N_{\delta Ped}$). Normalization is required. The normalization is performed relative to the stick limits imposed for each control, which is a unit-less number with a range of 0 to 1. In the case of rotors, the stick limits are from 0 to 5000 RPM, and for control surfaces they are from -15 to 15 degrees (30 degrees total).

The rudder commands have identical sensitivity, but for pedal commands the canted lifting rotors cause a much higher yaw authority than the uncanted version. The yaw control authority is about 300% higher in

hover and low speeds where the rudder lacks sufficient dynamic pressure to produce the necessary control moments. This is consistent with the observations from the ACS performed on the quadrotor configuration in the previous section.

These methods introduce the potential for low-order analysis of controllability considerations that can be used as constraints in conceptual design sizing and optimization, with lifting rotor cant angle as a relevant design parameter.

3.4. Safety

Cant can introduce several safety enhancements to the operation of an eVTOL aircraft. Cant can be used to position the rotor planes at angles that avoid intersection with pilot, passengers, critical subsystems or payloads. In the event of a blade break, the centrifugal force acting on the blade would not cause other systems to catastrophically fail if positioned appropriately. Although not specifically designed for in this study, the implications of this can be seen by comparing the rotors in Figure 2. Rotors inclined in the same direction will avoid the propagation of a blade break from one rotor to another.

If the wing, booms, and lifting rotors are positioned high on the fuselage, outboard canting of the anhedral configuration is preferable to reduce the risk of blade strike on the aircraft.

Another safety related implication of cant angles is the improved capability to maintain hover despite lateral wind shear. Lateral equilibrium of the uncanted configuration involves lateral control (δ_a) and roll attitude (ϕ) to balance the vehicles lateral forces and rolling moment, as shown in the first illustration of Figure 14. The greater the wind shear, the greater the lateral drag force on the vehicle, and the larger the roll angle must be to orient the thrust of the rotors to counteract it. This can be seen in Figure 15, which compares the roll attitudes of several configurations for trimmed hover with increasing lateral wind shear (negative v in a north-east-down coordinate system).

The typical multirotor definition of lateral-roll command is used in this case and is defined as follows (δ_a, or lateral control mode 1):

$$\delta_a = \Omega_3 + \Omega_4 + \Omega_7 + \Omega_8 + \Omega_{11} + \Omega_{12} - \Omega_1 - \Omega_2 - \Omega_5 - \Omega_6 - \Omega_9 - \Omega_{10} \quad (1)$$

Where Ω_n refers to the change in RPM (due to control variation) of rotor n, which are identified in Figure 2.

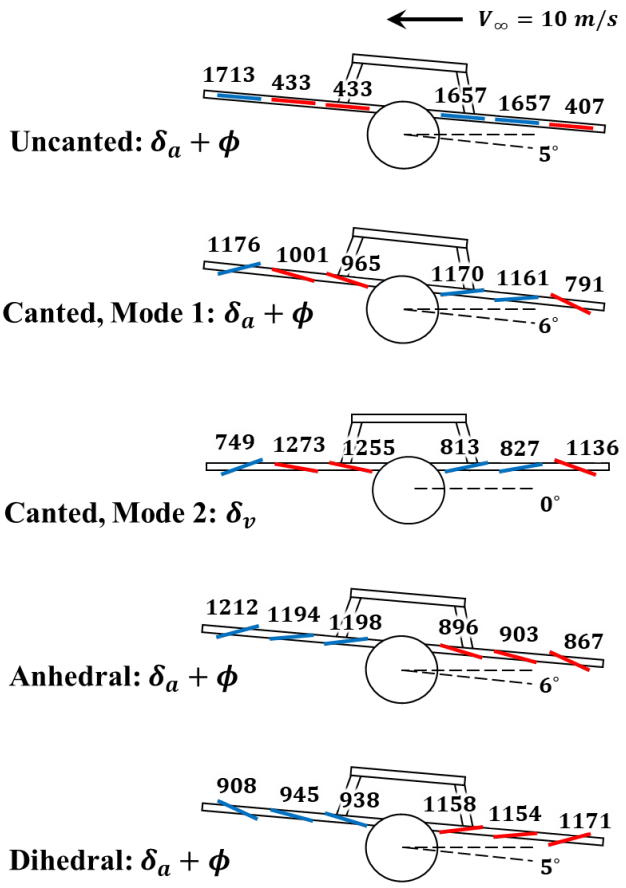

Figure 14: Front view of the aircraft showing control modes for lateral wind shear rejection with different cant angles.

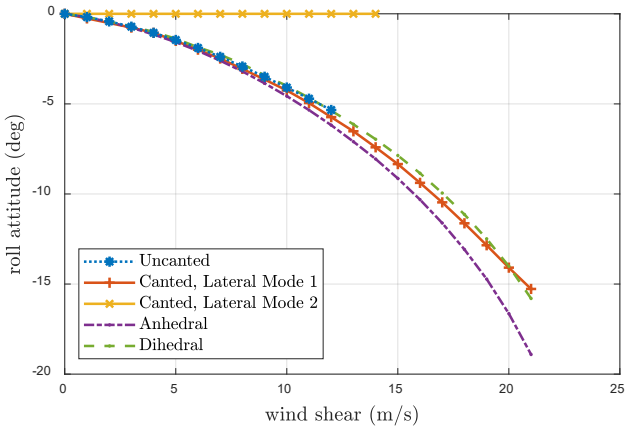

Figure 15: Trimmed roll attitude change with increased lateral velocity.

By this definition, a positive δ_a induces a roll-left attitude. Figure 15 shows that the lateral control mode 1 for both the canted and uncanted configurations requires high roll attitudes to hold a hovering position with significant lateral wind shear. This increases pilot

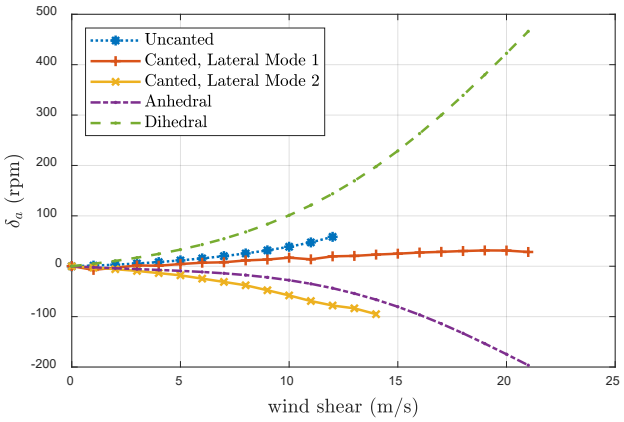

Figure 16: Trimmed differential lateral RPM control for increasing lateral velocity across three configuration/control methods.

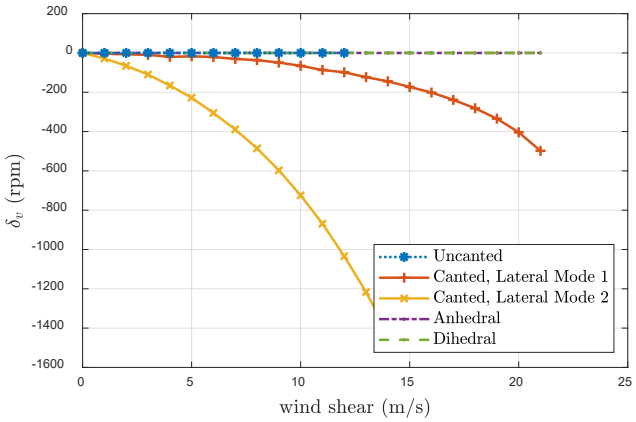

Figure 17: Trimmed differential outboard lateral RPM control for increasing lateral velocity across three configuration/control methods.

workload during critical landing and takeoff maneuvers and could possibly introduce a safety concern with wing-tip strike when hovering near the ground.

The canted configuration enables an additional independent control axis which is a differential outboard lateral control (δ_v, or lateral control mode 2). This lateral force control mode can be defined as follows:

$$\delta_v = \Omega_3 + \Omega_4 + \Omega_5 + \Omega_6 + \Omega_9 + \Omega_{10} - \Omega_1 - \Omega_2 - \Omega_7 - \Omega_8 - \Omega_{11} - \Omega_{12} \quad (2)$$

By this definition, positive δ_v increases the speed of the rotors canted in the direction of the pilot's left wing (see Figure 2), while decreasing the rotors canted to the pilot's right wing. The result is a net lateral force that can translate the vehicle decoupled from roll attitude. Introducing this control mode allows trim with zero roll attitude, as shown by the yellow line in Figure 15. Both modes can be used independently of each other to generate lateral forces, resulting in a bifurcation of the trim equilibrium into two local power minima, dominated by lateral mode 1 and lateral mode 2, respectively (Figure 14).

Further modifying the configuration to cant all rotors on one side of the wing in the same direction removes this independent control, as is the case for the anhedral and dihedral configurations (Figure 14). In these configurations, roll attitude is recoupled to lateral velocity, and control mode 2 is no longer independent of control mode 1.

Figure 16 and Figure 17 show the trimmed values of lateral (δ_a, lateral control mode 1) and differential outboard lateral (δ_v, lateral control mode 2) across lateral velocities and configurations. Large differential outboard lateral RPM adjustments must be used to trim with wing-level lateral translation due to the small cant

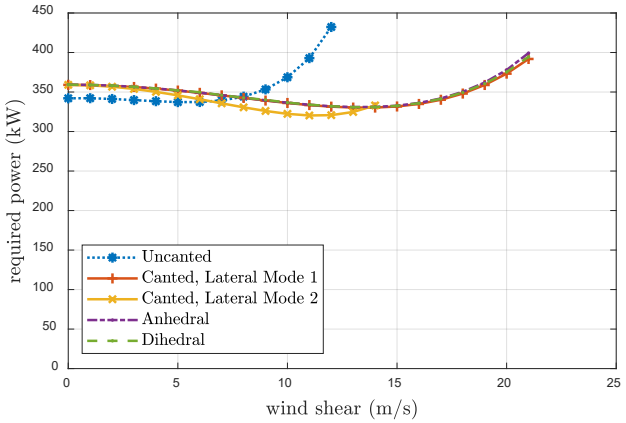

Figure 18: Trimmed power requirement with increased lateral velocity across three configuration/control methods.

angles. When allowed to trim with non-level wings (mode 1), the canted configuration can achieve trimmed hover with much higher lateral velocities before saturating the rotor speed (Figure 15).

This phenomenon has a secondary performance impact as well. These control methods have minimal impact on the power for low lateral velocities of up to 7 m/s, which can be seen in Figure 18. While the uncanted configuration hovers with marginally less power, it requires more power than a canted one for hovering with lateral winds over 8 m/s. This is shown in Figure 18. The canted configuration has the freedom of selecting control mode 1 or 2, either of which require less power than the canted case and can trim at velocities of up to 21 m/s, while the uncanted case is limited to 12 m/s.

3.5. Hover Stability

In addition to the previously mentioned impacts, reorientation of the lifting rotors will affect the stability

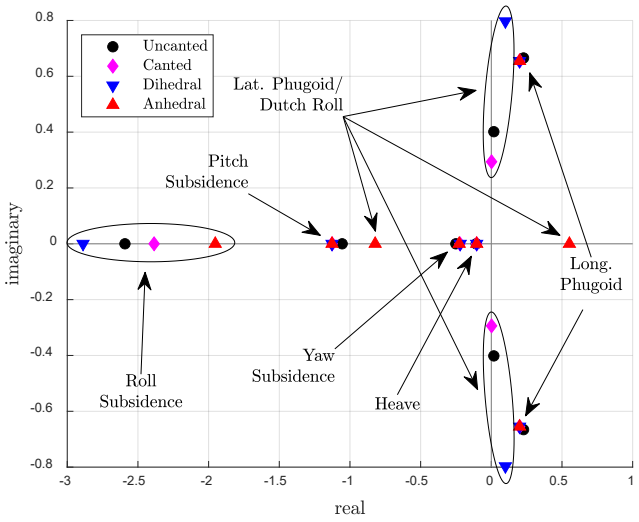

Figure 19: Eigenvalues of the stability derivative matrix in hover, showing characteristics of four different cant configurations.

characteristics of the aircraft, changing the damping and frequencies of the rigid body modes. As the rotor speed reduces to eventually lock the rotors for cruise, the impact of cant is diminished, so hover stability is deemed most consequential and examined more thoroughly below.

Figure 19 compares the eigenvalues of the stability matrix across the four illustrative configurations of Figure 2: (1) the uncanted configuration, (2) the canted configuration, (3) a dihedral cant configuration where rotors 5-12 in Figure 2 are mirrored across the centerline such that all rotors thrust towards the centerline, and (4) an anhedral cant configuration where rotors 1-4 are mirrored across the centerline such that all rotors thrust away from the aircraft centerline.

The dominant effect of introducing wing dihedral is to stabilize the roll subsidence mode. Here, this mode is stable for all four configurations shown in Figure 2 because of the high-wing position above the center of gravity. The dihedral cant angle increases the stability of this mode as shown in Figure 19, while the anhedral roll subsidence mode is the least stable. The canted configuration has two highly canted anhedral outboard rotor pairs and four moderately canted dihedral inboard rotor pairs. The net result is an intermediate roll stability between those of the dihedral and anhedral ones, most similar to the uncanted rotor in its stability characteristics.

The only remaining significant additional change in stability due to cant is in the lateral phugoid/dutch roll mode (which coincide in hover). Again, the fully anhedral and dihedral configurations deviate further, while canted and uncanted configurations are similar and in between these two extremes. Increased dihedral is observed to have a destabilizing effect on the lateral phugoid/dutch roll, while increasing the natural frequency of the mode. The pure anhedral configuration sees reduced frequency to the point that the mode becomes a pair of non-oscillatory lateral modes, one stable and one unstable.

3.6. Failure Tolerance

Depending on mission and certification requirements, an aircraft may need to be resilient to one or more thrust generator failure(s). A hypothetical example requirement is that in order to be authorized to fly and hover over populated areas, the aircraft must be resilient to two lifting rotor thrust failures. For the results shown in sections 3.6 and 3.7, the Lift+Cruise aircraft are sized to complete the mission shown in Figure 20, with a single or double rotor failure occurring during the final hover segment (the worst case condition). Note that Figure 20 describes the canonical sizing requirements for this aircraft and was originally generated in Ref. 1.

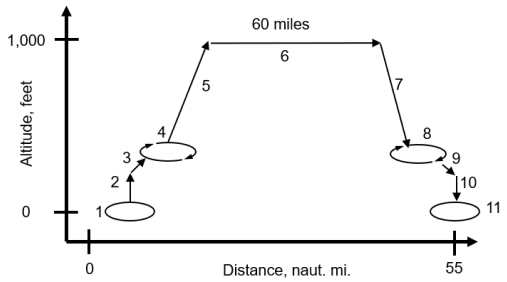

Segment	Type	time (min)	speed (m/s)	ROC (m/s)
1	Hover	0.5	0	0
2	Climb	0.08	0	2.54
3	Climb	0.52	28.29	2.54
4	Loiter	1	36.01	0
5	Climb	1.4	30.87	2.54
6	Cruise	32.73	49.18	0
7	Descent	1.4	30.87	-2.54
8	Loiter	1	36.01	0
9	Descent	0.52	28.29	-2.54
10	Descent	0.13	0	-1.52
11	Hover	0.5	0	0

Figure 20: Generic eVTOL mobility and delivery-type mission.

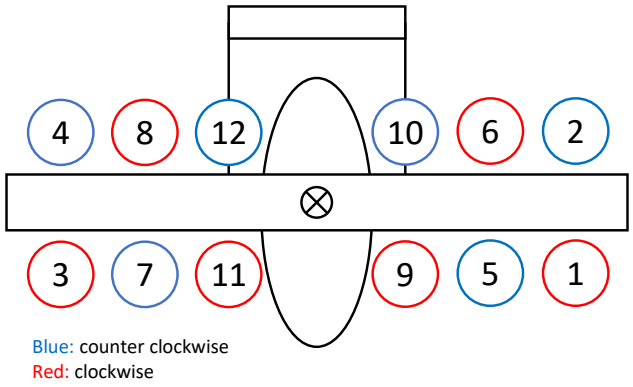

Figure 21: Alternate symmetrical configuration with "diametrically" (with respect to the aircraft center) opposite rotors turning in opposite directions.

In Ref. 2, a method for computing the best thrust redistribution in the case of thrust generator failures was presented. The method considers the most demanding flight case of maintaining hovering flight in the event of one or more lifting rotor thrust failures. The optimal redistribution of thrust for trim is computed such that the maximum thrust for any single rotor is minimized. Using this minimax method, the maximum torque and maximum power on the remaining rotors are also minimized.

For eVTOL configurations with all n lifting rotors thrusting in the same direction (no cant or tilt angle), a general result demonstrated in Ref. 2 is that the minimum ratio between the maximum thrust (T_{max}) for coping with the worst failure case of n_i inoperative lifting rotors is:

$$\left(\frac{T_{max}}{T_0}\right)_{Worst\ failure\ case} \geq \frac{n}{n-2n_i} \qquad (3)$$

This method was applied in Ref. 2 to the simplified version of the Lift+Cruise configuration with no cant angle on the aircraft's $n = 12$ lifting rotors. The choice of the direction of rotation of the 12 lifting rotors (see Figure 2) is not optimal (in terms of T_{max}/T_0) for coping with a double thrust failure. For $n_i = 2$ failed thrustors, the worst failure case is for any of the four pairs of adjacent lifting rotors turning in the same direction. Such a failure destabilizes the roll, pitch, and yaw axis and gives: $T_{max}/T_0 \sim 1.65$.

This thrust failure ratio can be lowered to the theoretical minimum:

$$\left(\frac{T_{max}}{T_0}\right)_{Worst\ failure\ case} = \frac{12}{12-4} = 1.5 \qquad (4)$$

by choosing the lifting rotors direction of rotation such that, with respect to the aircraft center, geometrically opposite rotors turn in opposite directions, as shown for example in Figure 21.

The optimal trim algorithm developed in Ref. 2 has been improved to deal with the canted cases. Hereafter are presented the results for the Lift+Cruise configuration (Figure 2) with and without canted lifting rotors. The most demanding failure conditions studied here are that the aircraft must be able to maintain hover despite one or two thrust failure(s) of any of the 12 lifting rotors. This is intended to provide a first estimate of maximum thrust, torque and power which are required in the early stages of predesign.

One Engine Inoperative Case

The One Engine Inoperative (OEI) case means that one lifting rotor is producing zero thrust as a result of some rotor or powertrain failure.

For the case with all cant angles equal to zero, the worst case is when one of the four outer lifting rotors (rotors 1, 2, 3, or 4) is in failure. This is because these rotors have the largest impact on roll control, having the longest lever arm with respect to the center of gravity. For pitch and yaw moments, all 12 lifting rotors have the same authority. The optimal trim in hover—minimizing the maximum thrust requirement to handle a worst-case OEI failure—is the same for hover at zero attitude angles or with free attitude angles. This means that the aircraft can maintain zero attitude angles in hover no matter which single rotor fails, but with a thrust ratio higher than the theoretical minimum which could be obtained by using the rotor rotational directions shown in Figure 21:

$$\left(\frac{T_{max}}{T_0}\right)_{OEI\ Worst\ failure\ case} = 1.25 > \frac{12}{12-2} = 1.2 \qquad (5)$$

For the case of canted rotors, the worst-case OEI failure is also for any of the four outer lifting rotors (rotors 1-4). In addition to being the rotors with the highest roll moment arm, they also have the highest cant angle (+/- 20°, see Figure 2), therefore a failed outer rotor has the highest destabilizing effect not only on roll, but also on the lateral and yaw axes. However, the result for the canted case in terms of $T_{max}/T_0 = 1.2504$ (Table 1) turns out to be close to the previous thrust ratio obtained for the uncanted configuration. The difference is that with canted rotors, trim at this thrust ratio is only possible if the canted configuration is allowed to have free roll and pitch attitude, whereas

the uncanted configuration has this relatively low thrust failure ratio by performing a horizontal hover trim even in OEI. Note that $T_{max,canted}$ for the canted configuration will still be higher than $T_{max,uncanted}$ for the same thrust ratio because $T_{0,canted} > T_{0,uncanted}$.

Two Engine Inoperative Case

The Two Engine Inoperative (TEI) case is when two lifting rotors produce zero thrust ($n_i = 2$). In this case, canted and uncanted configurations produce again the same lifting rotor selection for worst case TEI failure. The most stringent failure condition for both cases is when one of the four pairs of adjacent side-by-side lift rotors turning in the same direction fails, i.e. : one inner and one middle rotors on the same right or left side and on the same front or aft side, see Figure 2, rotors pairs: 5&9 or 6&10 or 7&11 or 8&12. This kind of double failure destabilizes four degrees-of-freedom in the uncanted case (vertical acceleration, roll moment, pitching moment and yaw moment) and five degrees-of-freedom in the canted case (the lateral axis acceleration in addition to the four previously mentioned).

The trim algorithm for finding the optimal thrusts redistribution on the 10 operating lifting rotors for this worst TEI failure has been applied both on canted and uncanted configurations either with free attitude angles or while imposing a horizontal attitude constraint. All the results of the failure analysis on these two Lift+Cruise configurations are presented in Table 1.

Table 1: Thrust ratios for the worst failures of 1 (OEI) or 2 (TEI) lifting rotors

		Canted	Uncanted	
	Failure	T_{max}/T_0	T_{max}/T_0	Theore. Min
Free Phi, Theta	OEI	1.2504	1.25	1.2
	TEI	1.6025	1.6524	1.5
Horiz. attitude	OEI	1.5134	1.2501	1.2
	TEI	2.3	1.6735	1.5

The highest thrust failure ratios are obtained for the most demanding condition—maintaining a horizontal hover despite a failure. Horizontal hover requires a very demanding thrust ratio of $T_{max}/T_0 = 2.3$ for the TEI on canted configuration. The uncanted version can achieve horizontal trim with minimal penalty to its T_{max}/T_0 ratio compared to the free phi/theta case. For the uncanted configuration, the horizontal trim is nearly optimal even with free attitude angles. In the following analysis, only the T_{max}/T_0 with free attitude angles will be considered, since it is a more realistic condition after a failure and in order to not penalize the canted configuration too much.

As a result of these additional degrees of freedom (hover with free pitch and roll angles), the thrust ratios for the canted configuration shown in Table 1 are less than or equal to the thrust ratios for the uncanted configuration. However, as with the OEI cases, even if the canted thrust ratio, T_{max}/T_0, is less than or equal to that of the uncanted configuration, the maximum required thrust $T_{max,canted}$ can be equal to or greater than $T_{max,uncanted}$ if $T_{0,canted} > T_{0,uncanted}$. For example, for the TEI case, although:

$$\left(\frac{T_{max}}{T_0}\right)_{canted} = 1.6 < \left(\frac{T_{max}}{T_0}\right)_{uncanted} = 1.65 \quad (6)$$

the ratio of their maximum thrust is close to one:

$$\left(\frac{T_{max,canted}}{T_{max,uncanted}}\right)_{TEI} = 1.0024 \quad (7)$$

This is not the case when imposing a hover with horizontal attitude constraint; in that instance the thrust failure ratios, T_{max}/T_0, are higher for the canted case. For example, for the TEI case, the maximum thrust with cant angles is about 42% higher than that of the uncanted case.

3.7. Failure Impact on Weight Assessment

The general approach, shared by the three tools (CREATION, NDARC, and HYDRA) for the weight estimates is as follows:

From the nominal lifting rotor hover thrust, T_0 and the thrust failure ratio T_{max}/T_0, the thrust, T_{max} was computed and used for the estimation of some the subsystem weight models (e.g., wing weight, booms weight). Furthermore, the ratio of maximum required power to the nominal power (without failure) for the worst failure case is:

$$\frac{P_{max}}{P_0} = \left(\frac{T_{max}}{T_0}\right)^{\frac{3}{2}} \quad (8)$$

This relation stems from the fact that the induced power is the predominant term of required power in hover and induced power varies as $P \sim Thrust^{3/2}$ (a well-known result in momentum theory). This ratio, P_{max}/P_0, along with P_0, the largest nominal lifting rotor power value in hover, were used to calculate P_{max}. This maximum required power P_{max} was then used to

size the electric powertrain components of the lifting rotors.

3.7.1 Electric motor and ESC weight models

The three tools: CREATION, NDARC, and HYDRA possess separate electric motor and electronic speed controller (ESC) weight models such that, even for identical P_0 and P_{max}/P_0, motor and ESC weight estimates differ. As documented in Ref. 1, power and weight estimates for each tool differ as well. In this section, the details of the electric motor and ESC weight models are discussed so that context can be given to the failure case total weight assessments to follow.

In CREATION, the simplest motor and convertor weight model available was used to ease the interpretation of the results and is shown below.

$$W_{motor+Convertor} = (1 + MassPenalty) \times \left(\frac{1}{PowerDensity_{Motor}} + \frac{1}{PowerDensity_{convertor}} \right) \times P_{max} \quad (9)$$

where weights are in kg and power in W.

The "MassPenalty" term accounts for the weight installation of the motors on the aircraft compared to the standalone weight. For the lifting motors, the equivalent power density in terms of mass has been assumed to be 6 kW/kg and the associated convertors is 17kW/kg. For comparison, this is slightly higher than that of an Emrax228 moor, which is about 4.8~5.2kW/kg depending on the cooling system. For the Cruise Motor driving the pusher propeller, the equivalent power density is 5.12 kW/kg in CREATION (as for an Emrax348). A "MassPenalty" factor of .3 was assumed for each.

NDARC possesses a variety of models for motor and speed controller weight estimation. For this research effort, a torque-based regression derived from publicly available data on the Emrax series of motors was used (Ref. 15). The model is reproduced below.

$$W_{motor} = 0.1123 Q_{peak} + 7.8378 \quad (10)$$

Q_{peak} is in ft-lb and W_{motor} is in lb. Nominal lifting rotor RPM for the NDARC model in hover at the DGW was 3200, corresponding to a lifting rotor tip speed of 680 ft/s. The speed controller model used for this paper is from Ref. 16 and shown below, where W_{esc} is in lb and P_{max} is in horsepower.

$$W_{ESC} = 0.20792 * P_{max}^{.96} \quad (11)$$

For the current work, HYDRA used an empirical fit of Launchpoint and Emrax electric motor weights combined with manufacturer-recommended (Ref. 17) ESC weights which gives the total motor+ESC weight as a quadratic function of maximum continuous power:

$$W_{motor+esc} = -8.836(10^{-4}) P_{max}^2 + 0.582 P_{max} \quad (12)$$

where $W_{motor+esc}$ is in lb and P_{max} is in horsepower. For a typical sizing task, P_{max} would be the maximum continuous power required by the motor for a given mission. For the current failure analysis, P_{max} is calculated with Equation 8 using the thrust ratio values from Table 1. For context, the model shown in Equation (10) predicts $W_{motor+esc} = 12.12\ kg$ for $P_{max} = 37\ kW$, corresponding to an Emrax188AC motor (7.5 kg) and BAMOCAR-D3 speed controller (5.8 kg) total mass of 13.3 kg. For $P_{max} = 56\ kW$, $W_{motor+esc} = 17.58\ kg$ corresponding to an Emrax208AC motor (9.4 kg) and BAMOCAR-D3 controller (5.8 kg) total mass of 15.2 kg. Both $P_{max} = 37\ kW$ and $P_{max} = 56\ kW$ are typical power requirements for the current work.

3.7.2 Design Gross Weight Comparison

In this section, cases of one (OEI) or two (TEI) lifting rotor thrust failures are compared with the ideal case of no failure (AEO). The results of the sizing loop were first compared in terms of Design Gross Weight (DGW) obtained by CREATION, NDARC, and HYDRA. In the following sections, only results for free phi and theta (aircraft attitude angles) are shown. The reason for not including horizontal attitude (attitude angles equal to zero) constraints is that T_{max}/T_0 and P_{max}/P_0 increased to such a degree that convergence issues were experienced for some of the tools.

This and subsequent sections use the following definitions: 1) *All Engines Operative (AEO)* – This is a theoretical utopic case for comparison where no thrust generator failure is accounted for. For these cases, the weight assessments were performed with $T_{max}/T_0 = 1$. The AEO calculations serve as a reference to assess the impact of failures. 2) *One Engine Inoperative (OEI)* – One outer lifting rotor failure (rotors 1, 2, 3, or 4 in Figure 2). Thrust ratios for OEI cases are shown in Table 1. 3) *Two Engines Inoperative (TEI)* – One of the four pairs of two adjacent lift rotors turning in the same direction are in failure (see Figure 2). Thrust ratios for TEI cases are shown in Table 1. Fallout design gross weight results are shown in Table 2 for each set of failure cases for

canted and uncanted configurations and compared by tool.

For all three codes, the trend with respect to canted vs uncanted configurations is that despite a higher maximum thrust ratio T_{max}/T_0 =1.6524 for the TEI uncanted configuration compared to T_{max}/T_0 =1.6025 for the TEI canted configuration (see Table 1), the DGW values are relatively close—the TEI canted result was only slightly greater than the TEI uncanted result computed by the same code. This is because the nominal T_0 and P_0 of the canted case were higher than in the uncanted case (because the thrust vector is not directly vertical) resulting in similar values of T_{max} and P_{max}. Those values were then used in CREATION, NDARC, and HYDRA to calculate electric motor and ESC weight as well as wing and boom weights resulting in the general trend of $DGW_{canted} > DGW_{uncanted}$ seen in Table 2.

Subsystem weight models (particularly the electric motor and ESC weight models) drove the increase in DGW as number of failed rotors increased. Higher values of P_{max} resulted in increased motor and ESC weight, which in turn increased the GTOW of the vehicle associated subsystems. Since the mass-performance loop is an iterative process, this results in a larger converged DGW. A complete subsystem weight breakdown for all the cases shown in Table 2.

Table 2: Design Gross Weight results for CREATION, NDARC, and HYDRA for AEO, OEI, and TEI cases, in kilograms.

DGW (kg)		CREATION	NDARC	HYDRA
AEO	CANTED	1141	1211	1109
	UNCANTED	1115	1196	1084
OEI	CANTED	1309	1278	1137
	UNCANTED	1262	1259	1101
TEI	CANTED	1458	1444	1229
	UNCANTED	1428	1433	1207

Comparing the results in Table 2 by code, CREATION has the largest increase in DGW when introducing rotor failure, followed by NDARC, and then by HYDRA. Because the computed values of T_{max} and P_{max} depend only on the AEO thrust and power, starting out at a lower AEO DGW (assuming all codes predict similar hover P_0 and T_0 for a given DGW, which has been shown to be a good assumption in Ref. 1) will result in a smaller cascading weight effect as T_{max}/T_0 is increased. NDARC predicted the heaviest AEO weight among the tools utilized and closely resembled CREATION's weight estimates for the OEI and TEI failure criteria. Recall from Ref. 1 that NDARC and HYDRA incorporated traditional component-level margins as an allocation for potential failure cases-these allocations were maintained in the AEO case. These are first-order observations which are explored in more detail in the following section.

3.7.3 Subsystem Weight Breakdown

In order to further understand the effect of a single or double rotor/motor failure on vehicle sizing, a complete subsystem weight breakdown is presented. Figure 22 shows the weight breakdown for all three tools for the canted configuration, while Figure 23 shows analogous results for the uncanted configuration. In Figures 22 and 23, the AEO, OEI, and TEI failure cases are shown side-by-side. Organizing the data in this manner shows how subsystem weights change with increasing T_{max}, P_{max}, and DGW.

For this study, aircraft component dimensions were fixed. As a result, the weight of the rotors do not change; the rotor weight estimation methods used by CREATION, NDARC, and HYDRA are functions of geometry, and in some cases, blade flapping frequency. For both HYDRA and NDARC, the AFDD00 rotor weight model was used with an assumed flapping frequency of 1.25/rev (Ref. 18). In addition to the rotor model, other component weights fell into two categories:

a) Components for which weight estimates directly vary with the gross weight and for which the relative weight is insensitive to failure criteria, including landing gear, fuselage, vibration, and other systems;

b) Components for which the relative weight is directly dependent on the failure condition, including the wing, booms, empennage, motor and battery systems.

The first group of components were not as important for analyzing the impact of failure criteria on vehicle weight; even though there were small variations in $W_{subsystem}/DGW$, the higher thrust and power requirements of the failure cases do not impact these subsystem weights directly, only indirectly via an overall increase in DGW.

The second group of components are dependent on power requirements. These components are more sensitive to changes in failure condition.

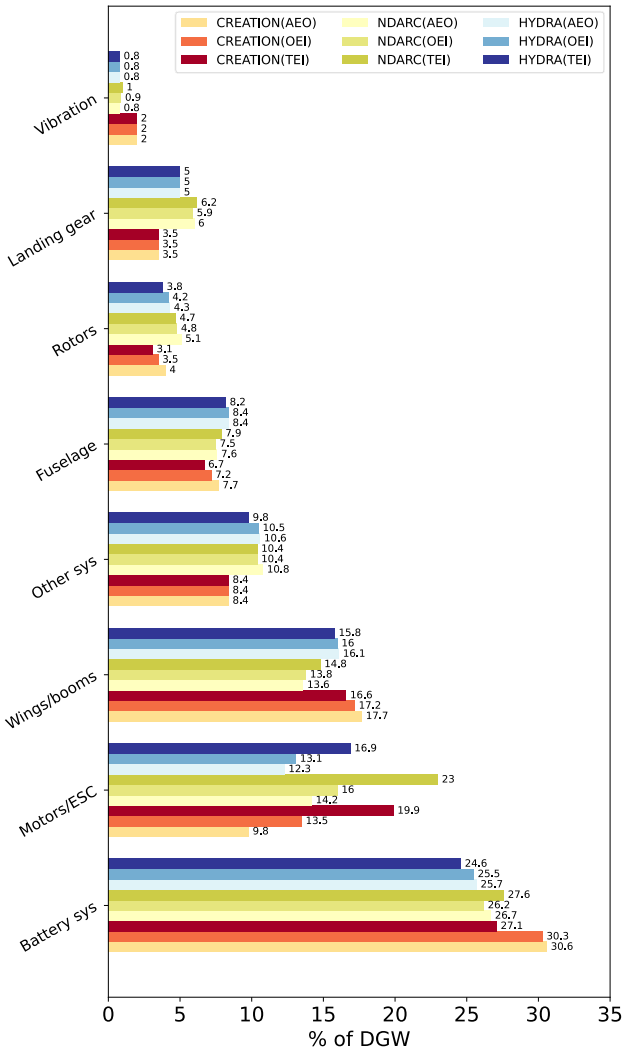

Figure 22: Subsystem weights as a percentage of DGW for the uncanted configuration.

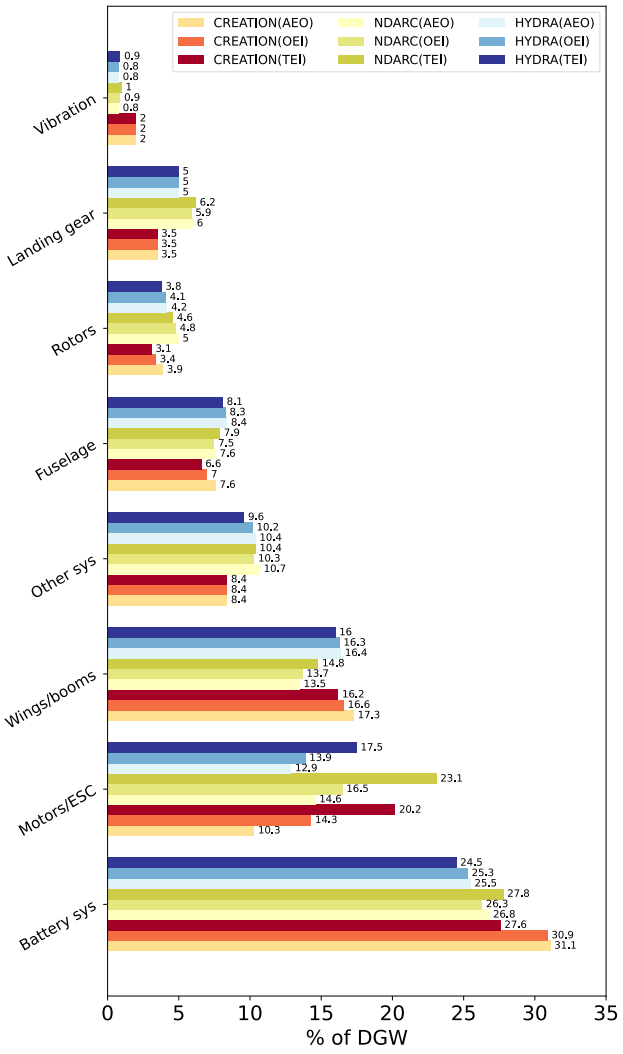

Figure 23: Subsystem weights as a percentage of DGW for the canted configuration.

Computed DGW values were higher for canted rotors (Table 2). In terms of contribution to the DGW (Figure 22 and 23), the component weight fractions were very close between the canted and uncanted versions of the L+C considered here. Only a slight increase on the percentages of weights of the second group was observed.

Understanding the interdependency of all the components weights within the "Mass-Performance" loop is critical in interpreting these results. If a weight model (e.g. the motor) when queried separately gives a higher weight (e.g. HYDRA motor weight model compared to the CREATION model) than another one for the same input (see for AEO cases: Wmotor_Hydra > Wmotor_Creation), this may change when considering a case (OEI or TEI) where the input (Pmax) becomes higher due to the increased growth of other components.

Focusing on the second group, which corresponds to the most important drivers of the failure impact on weight, deeper insights can be obtained by considering the ratios of each of these component weights with respect to their associated values for the AEO case (canted or uncanted, see Figure 24 – 26), i.e.:

$$W_{Component,\ OEI\ or\ TEI}\ /W_{Component,\ AEO}$$

Wing and Booms

Figure 22 and Figure 2023 show that the trends in wing/boom mass with respect to the AEO, OEI, and TEI cases were very close between CREATION and HYDRA. For these tools, there was a small decrease in $W_{wing/booms}/DGW$ for increasing number of failed rotors. Although the wing and boom weights increased with T_{max} for both codes, the increase in motor/ESC weight drives up the DGW at a faster rate. NDARC's model resulted in higher

$W_{wings/booms}/DGW$ with increasing number of failed rotors. For the wing and booms weights:

- CREATION used T_{max} as a structural constraint for sizing; the T_{max} constraint was applied depending on each boom's position along the wingspan. T_{max} was applied depending on the positions of the 2 lifting rotors on each boom.
- NDARC wing and boom weight models do not natively possess a sensitivity to changes in T_{max}. For this study, NDARC's calibration factor for the default wing weight equation (AFDD93) was modified to account for increases in bending stress using the relative sensitivity of the regression to this parameter (Ref. 18). This change involved computing the relative bending stress from the failure condition compared to a pure elliptically loaded wing assuming simple beam bending theory; this bending stress ratio was raised to the power of 1.2 (computed from the exponents related to the structural design gross weight and aspect ratio) and incorporated into the calibration factor of the AFDD93 regression.
- HYDRA used the AFDD93 weight model for the wing, with modifications to account for flap and boom weight. The HYDRA model assumed that rotor loads were evenly distributed over the wing. In nominal conditions (AEO), maximum loads on the wing occur during the vertical climb segment (see Figure 18) due to the additional total thrust required compared to hover. But for the failure conditions (OEI, TEI) the maximum thrust loads T_{max} on wing and booms were applied to the hover case.

Figure 24 shows that the percentage increase in wing and boom weight in comparison to the AEO reference cases. Relative weight increase between CREATION and NDARC for the wing and booms was close: a variation of +7 to 10% for the OEI case and about 20% for the TEI case. Weaker impacts were observed in HYDRA (+1~2% in OEI and +8~9% for the TEI case).

Battery Systems

Battery system weight accounted for between 25.5 and 31.1% of the DGW (see Figure 22 and 23). CREATION predicted a battery system weight fraction of 31.1% (with respect to DGW) for the canted AEO case, compared to 26.8% for NDARC and 25.5% for HYDRA. For the OEI canted and uncanted cases CREATION, NDARC, and HYDRA battery weight

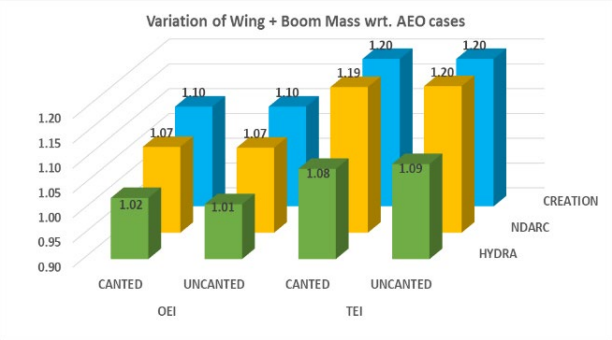

Figure 24: Wing and boom weights ratios with respect to the corresponding AEO weights.

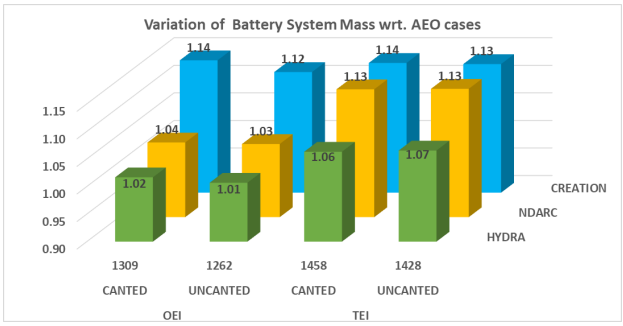

Figure 25: Battery system weights ratios with respect to the corresponding AEO weights.

fraction remained similar. However for the TEI cases both HYDRA and CREATION battery weight fraction decreased while NDARC's increased slightly. As shown in Table 2, HYDRA's DGW estimate was lower than NDARC and CREATION, especially for the OEI and TEI cases. This was in part due to cascading weight impacts via nonlinear weight model sensitivities. CREATION shows a large drop in battery weight fraction when comparing the TEI case to the OEI case and corresponding large jump in motor+ESC weight fraction. The variation of battery system mass normalized by the AEO battery mass was again very similar between the canted and uncanted versions for each tool (see Figure 25).

For the OEI case, HYDRA and NDARC both predicted a small increase of about 1~4%, whereas CREATION yielded a larger increase of 13% with respect to the AEO case. For the TEI case the same result was obtained (+13% of increase) by CREATION and NDARC, while HYDRA predicted a 5% difference. These relative changes in battery mass appeared to correlate with increases in gross weight (see Table 2). Notice that the step change between the OEI and TEI battery system weight was not present in the CREATION results ; this is because for the

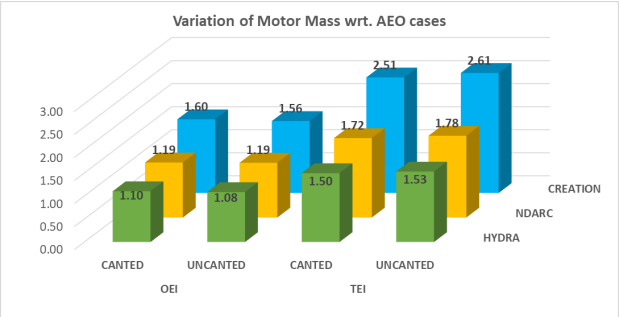

Figure 26: Motors and ESC weights ratios with respect to the corresponding AEO weights.

TEI case, the wing flaperon was deflected which offset some of this power increase. Without this change in flaperon setting for the CREATION model, the battery system mass increased such that the sizing loop diverged.

Motor/ESC - The most significant differences in Figure 26 appear in the motor/ESC weight computations, not only between the AEO, OEI, and TEI cases, but also to the extent in which rotor failure affected the weight prediction methods. In this study, motor and ESC weight were strongly influenced by OEI and TEI requirements. For all three tools, motor weight was directly dependent on P_{max} (see Section 3.71). From Equation 8 and the T_{max}/T_0 ratios from Table 2, the corresponding power ratios were $P_{max}/P_0 \approx 1.40$ for both canted and uncanted OEI cases. TEI power ratios were $P_{max}/P_0 \approx 2.03$ and $P_{max}/P_0 \approx 2.12$ for the canted and uncanted cases respectively. This is why for both canted and uncanted cases, all codes show a relatively smaller increase in Motors &ESC weight for the OEI case, and a much larger increase for the TEI case.

The ratios of maximum power increase required to cope with OEI and TEI failure criteria have different effects depending on the motor and ESC weight models described in Section 3.7.1. For example, within CREATION, the model used here depends linearly on the maximum power with a specific power for each kind of electric motor. Other cumulative weight growth causes a "snow ball effect", increasing the relative weight of these components and overall mass grows

NDARC and HYDRA motor and ESC weight models exhibit a smaller (apparently) quadratic sensitivity vs. number of failed lifting rotors. NDARC used a linear torque-based parametric for motor weight and nearly linear power-based parametric for speed controller weight. HYDRA utilized a quadratic model for motor and speed controller weight, with a comparably small quadratic term. Note that the motor weight model used in NDARC possessed a zero-intercept term.

Motor+ESC estimates are closer when considering the weight percentage variation relative to DGW (Figure 22 and Figure 24). Results below are for the canted configuration. Note that, when comparing the equivalent failure case, NDARC's combined motor and ESC weight fraction were higher than both CREATION or HYDRA's (see Figure 22 and Figure 24).

- CREATION's Motor/ESC weight fraction with respect to DGW increased from ~0.1 to ~0.2 from the AEO to TEI case, corresponding to a non-normalized weight increase of $W_{Motors\ \&\ Esc(TEI)} - W_{Motors\ \&\ Esc(AEO)} = 294 - 117 = 177\ kg$
- NDARC's Motor/ESC weight fraction increased from ~0.14 to ~0.23, corresponding to a non-normalized weight increase of $W_{Motors\ \&\ Esc(TEI)} - W_{Motors\ \&\ Esc(AEO)} = 304 - 176 = 128\ kg$.
- HYDRA's Motor/ESC weight fraction increased from ~0.12 to ~0.17, corresponding to a non-normalized weight increase of $W_{Motors\ \&\ Esc(TEI)} - W_{Motors\ \&\ Esc(AEO)} = 214 - 143 = 71\ kg$.

CONCLUSIONS

The complexity of predesign studies for emerging eVTOL aircraft that possess both rotary and fixed wings has been illustrated by considering the pros and the cons of using canted lifting rotors from different technical perspectives.

The most important positive effects are:

1) The increase of yaw authority in hover and low speeds as well as an improved lateral relative wind capacity;
2) The direction of cant (dihedral, i.e. inboard, or anhedral, i.e. outboard) can be chosen for safety reasons; for reducing blade strike risks on the airframe or other lifting components;
3) The dominant effect of introducing dihedral on the lifting rotors is to increase the stability of the roll subsidence mode in hover and low speeds.

Useful results were observed from the study of the lateral relative wind capability. Using lifting rotors canted in opposite directions on the same right/left side of the aircraft (as the example L+C configuration studied here) allows lateral translation with horizontal

attitude. Such configurations can sustain lateral relative winds with no or reduced roll angle. Dihedral cant effects are additive with respect to rotor lateral forces and roll moments, whereas anhedral cant has subtractive effects requiring the highest roll angles for sustaining lateral winds.

Negative impacts are an increase in thrust, torque and power for hovering, climbing and other vertical maneuvers in VTOL flight. Note that the positive effects of canting can be obtained with low cant angles. This increase in thrust and power demand with cant angles has an effect on the design gross weight which is reinforced if a hover safety condition with rotor failure is imposed. However, if this demanding condition is relaxed by allowing non-zero attitude angles in hover for rotor-out conditions, the canted configuration shows similar DGW growth compared to the uncanted configuration.

From a vehicle sizing perspective, the following conclusions can be drawn based on the results presented in sections 3.6 and 3.7:

1) Choice of electric motor weight model is important for conceptual design and the importance is multiplied when sizing a vehicle to handle one or more rotor/motor failures. Models should be calibrated to match the power, torque, and angular velocity requirements of each study.

2) When sizing for failure cases, careful evaluation of safety and other requirements to avoid oversizing motors or other powertrain components is prudent. For example, allowing non-zero attitude angles in hover or permitting motors to operate in an emergency condition at higher than maximum continuous rated power can substantially relieve weight penalties when imposing these conditions.

3) While “safety through redundancy” is a natural approach for the design of eVTOL aircraft, there are associated weight penalties and specific failure cases which must be carefully evaluated early in the predesign/conceptual design process to determine the performance tradeoffs

Further studies on rotor/rotor and rotor/wing aerodynamic interactions, as well as in ground effect disturbances, particles projection, brown-out, Vortex Ring State etc. are needed for a next step level of investigation towards a more comprehensive holistic approach.

Author contact:

Pierre-Marie Basset: Pierre-Marie.Basset@onera.fr

Jean-Paul Reddinger:
jean-paul.reddinger-ext@onera.fr

Raphaël Perret: Raphael.Perret@onera.fr

4. REFERENCES

1. Vegh, J.M, Basset, P.-M., Beals, N., Scott, R., Perret, R., Singh, R., “A comparison of three conceptual design approaches applied to an electric distributed lift aircraft”, 49th European Rotorcraft Forum, Bückeburg, Germany, September 2023.

2. Basset, P.-M., Perret, R., “Failure Analysis Method for the Presizing of Multi-Rotors eVTOL”, 48th European Rotorcraft Forum, Winterthur, Suisse, 6-9 September 2022.

3. Basset, P.-M., Tremolet, A., Beaumier, P., Rakotomamonjy, T., *“CREATION: a numerical workshop for rotorcraft concepts generation and evaluation”*, Rotorcraft Virtual Engineering Conference, Liverpool, 8-10 Nov. 2016.

4. Basset, P-M., Tremolet, A., Cuzieux, F., Schulte, C., Tristrant, D., Lefebvre T., Reboul, G., Costes, M., Richez, F., Burguburu, S., Petot, D., Paluch, B., “The C.R.E.A.T.I.O.N. project for rotorcraft concepts evaluation: The first steps”, 37th European Rotorcraft Forum, Gallarate, Italy, 13-15 September 2011.

5. Basset, P.-M., Tremolet. A., Bartoli, N., Lefebvre, T., “Helicopter presizing by multidisciplinary – multi objective optimization,” OPT-i 2014, International Conference on Engineering and Applied Sciences Optimization, M. Papadrakakis, M.G. Karlaftis, N.D. Lagaros (eds.), Kos Island, Greece, 4-6 June 2014.

6. Johnson, W., “NDARC — NASA Design and Analysis of Rotorcraft, Theoretical Basis and Architecture,” American Helicopter Society Specialists' Conference on Aeromechanics. San Francisco, CA, January 2010.

7. Johnson, W., "Technology Drivers in the Development of CAMRAD II," American Helicopter Society Aeromechanics Specialist Meeting, San Francisco, CA, January 1994.

8. Vegh, J.M., Botero, E., Clarke, M., Smart, J., and Alonso, J., “Current Capabilities and Challenges of NDARC and SUAVE for eVTOL Aircraft Design

and Analysis", AIAA Propulsion and Energy 2019 Forum, Indianapolis, IN, 2019, https://doi.org/10.2514/6.2019-4505.

9. Johnson, W., and Silva, C., "Observations from Exploration of VTOL Urban Air Mobility Designs," Seventh Asian-Australian Rotorcraft Forum, Jeju, Korea, 2018.
10. Sridharan, A., Govindarajan, B., Nagaraj, V., and Chopra, I., "Design Considerations of a Lift-Offset Single Main Rotor Compound Helicopter," American Helicopter Society Aeromechanics Design for Vertical Lift, San Francisco, CA, January 20-22 2016.
11. Govindarajan, B., Sridharan, A., and Avera., M., "Integration on Physics Based Weight Models into Rotorcraft Design Sizing," 43rd European Rotorcraft Forum, Milan, Italy, September 12-15 2017.
12. Beals, N., and Govindarajan, B., "Trim Strategies for Over-Actuated Vehicle Configurations During Conceptual Design," AIAA Aviation 2021 Forum, Virtual Event, August 2-6 2021.
13. Juhasz, O., Reddinger, J.P., Whitt, J., "System Identification of a Hovering Quadrotor Biplane Tailsitter with Canted Motors," Proceedings of the Vertical Flight Society, Montréal, QC, Canada, May 2024.
14. Atci, K., Jusko, T., Štrbac, A. et al. "Impact of differential torsional rotor cant on the flight characteristics of a passenger-grade quadrotor." *CEAS Aeronaut J* (2024).
15. Chen, G., Vegh, J.M., and Milligan, A., "An Investigation into the Electrification of an Advanced Tiltrotor Concept," AIAA Aviation Forum, San Diego, CA, June 2023, https://doi.org/10.2514/6.2023-3842.
16. Duffy, M., Sevier, A., Hupp, R., Perdomo, E., and Wakayama, S, "Propulsion Scaling Methods in the Era of Electric Flight," 2018 AIAA/IEEE Electric Aircraft Technologies Symposium, AIAA Paper No. 2018-4978, July 2018, https://doi.org/10.2514/6.2018-4978.
17. User's Manual for Advanced Axial Flux Synchronous Motors and Generators", EMRAX Innovative E-Motors, www.emrax.com/wp-content/uploads/2017/01/user_manual_for_emrax_motors_january_2017_version_4.5.pdf
18. Johnson, W., "NDARC. NASA Design and Analysis of Rotorcraft Theory," NASA/TP–20220000355/Vol 1, 2022.